Journal of Materials Chemistry

Dynamic Article Links

Cite this: *J. Mater. Chem.*, 2011, **21**, 19030

www.rsc.org/materials

PAPER

Ultrasensitive ratiometric fluorescent pH and temperature probes constructed from dye-labeled thermoresponsive double hydrophilic block copolymers†

Jinming Hu, Xiaozheng Zhang, Di Wang, Xianglong Hu, Tao Liu, Guoying Zhang* and Shiyong Liu*

Received 27th July 2011, Accepted 22nd September 2011
DOI: 10.1039/c1jm13575a

We report on the fabrication of highly sensitive ratiometric fluorescent pH and temperature probes based on thermoresponsive double hydrophilic block copolymers (DHBCs) with the two blocks labeled with two types of dyes possessing different pH-switchable emission characteristics. P(NIPAM-*co*-FITC)-*b*-P(OEGMA-*co*-RhBAM) DHBCs were synthesized *via* consecutive reversible addition–fragmentation chain transfer (RAFT) polymerizations in combination with post-modifications, where NIPAM, OEGMA, FITC, and RhBAM are *N*-isopropylacrylamide, oligo(ethylene glycol) monomethyl ether methacrylate, fluorescein isothiocyanate, and rhodamine B-based derivatives, respectively. Due to that FITC and RhBAM moieties exhibit prominent decrease and increase in emission intensities with decreasing solution pH, respectively, intensity ratios of characteristic RhBAM and FITC emission bands, I_{582}/I_{522}, of P(NIPAM-*co*-FITC)-*b*-P(OEGMA-*co*-RhBAM) unimers at 25 °C exhibit ~39-fold changes in the range of pH 2–10. At elevated temperatures, thermo-induced formation of PNIPAM-core micelles enables effective fluorescence resonance energy transfer (FRET) between FITC and RhBAM moieties respectively located within micellar cores and coronas, and I_{582}/I_{522} exhibits ~52.5-fold changes in the same pH range. The reported dually modulated multicolor-emitting P(NIPAM-*co*-FITC)-*b*-P(OEGMA-*co*-RhBAM) DHBCs are capable of ultrasensitive fluorometric detection of solution pH and temperature in a ratiometric manner, which augurs well for their practical applications in sensing, imaging, and the fabrication of new generation of theranostic systems.

1. Introduction

During the past two decades, increasing attention has been paid to stimuli-responsive block copolymers.[1–10] They typically undergo reversible or irreversible changes in physical properties and/or chemical structures and self-assembled nanostructures to an external stimulus such as pH, temperature, ionic strength, mechanical forces, light irradiation, electric and magnetic fields, and specific analytes or a combination of them. Their applications in diverse fields ranging from drug and gene delivery, tissue engineering, to chemosensors and biosensors have also been extensively explored.[11–26] Recent research efforts in this area have focused on the development of novel responsive block copolymers integrated with multiple functions (*e.g.*, targeted drug delivery and optical sensing/imaging) and those possessing high sensitivity, and reactivity towards specific biological milieu such as pathological tissues, cancer cells, and certain organelles.[27–32]

For example, in living organisms, pH and temperature play key roles on the cell and tissue activities, and pathological processes and dysfunctions are typically associated with abnormal pH and temperature variations.[33–36] Certain tumor tissues and organs possess lower extracellular pH (~6.0–6.5) compared to normal ones (pH 7.2–7.4) and pathological cells might have higher temperatures than normal ones due to enhanced metabolic activities.[37–40] In addition, intracellular pH gradients also exist, ranging from pH 5.9–6.2 in early endosomes to pH 5.0–5.5 in late endosomes and lysosomes.[29,41] Thus, the accurate monitoring of pH gradients and temperature variations is quite critical for the diagnosis of certain diseases, the determination of pathogenesis, the tracing of intracellular transport pathways of drug nanocarriers, and the measurement of therapeutic efficiencies.

The fluorometric technique is simple to perform and offers the high sensitivity required especially when measuring changes in small dimensions at the nanometre scale.[30,42–56] During the past decade, quite a few polymeric fluorescent pH probing systems have been developed. In 2004, Uchiyama *et al.*[57] synthesized multi-responsive copolymers labeled with a polarity-sensitive dye (DBDAE); due to that the thermo-induced phase transition temperature is highly dependent on pH, the reported dye-labeled random copolymer can serve as fluorescent pH and temperature

CAS Key Laboratory of Soft Matter Chemistry, Department of Polymer Science and Engineering, Hefei National Laboratory for Physical Sciences at the Microscale, University of Science and Technology of China, Hefei, Anhui, 230026, China. E-mail: sliu@ustc.edu.cn; gyzhang@ustc.edu.cn

† Electronic supplementary information (ESI) available: supplementary Table S1 and Figs S1–S6. See DOI: 10.1039/c1jm13575a

probes by monitoring changes in DBDAE emissions. Hoogenboom and coworkers[58] fabricated a polymeric pH and temperature sensor based on disperse red 1 (DR1)-labeled thermoresponsive polymer. Just recently, Gao *et al.*[31] successfully fabricated ultrasensitive pH probes based on double hydrophilic block copolymers (DHBCs) consisting of poly(ethylene oxide) (PEO) and tetramethyl rhodamine (TMR)-labeled poly(tertiary amine methacrylate) blocks. The critical micellization pH can be adjusted by varying the *N*,*N*-dialkyl substituent. In the micellar state, the TMR emission was almost switched off due to the close proximity of TMR residues within micellar cores and PET effect of tertiary amine moieties. Below the pK_a of pH-responsive block, micelle-to-unimer transition occurs and is accompanied with the effective "turn-on" of fluorescence emission. It should be noted that the above three examples of polymeric pH probes are all based on changes of a single emission band, which might exhibit inherent limitations such as high background interference, less satisfactory repeatability, and decreased reliability due to fluctuations in complex detection conditions. Thus, it is highly desirable to develop ratiometric fluorescent pH and temperature probes by simultaneously monitoring the intensity of two emission bands to achieve improved sensing performance *via* the self-calibration effect.

In this context, ratiometric fluorescent pH probes based on the fluorescence resonance energy transfer (FRET) principle or the introduction of an internal reference dye have been designed. In a typical example, Krishnan *et al.*[29] reported a pH-triggered DNA nanomachine labeled with FRET donor and acceptor at the two terminals. The mapping of spatial and temporal pH gradients within living cells was achieved due to the conformational transition of a DNA I-switch between "open" and "closed" states in the narrow pH range of 5–7. Jo *et al.*[59] labeled pH-responsive poly(sulfadimethoxine methacrylamide) (PSDM, pK_a ~ 7) with pyrene and coumarin 343 dyes at the diblock junction point and chain terminals, respectively. The variation of solution pH below and above 7 leads to chain collapse/aggregation and swelling, respectively, resulting in enhanced or decreased FRET efficiencies.

The above two nice examples take advantage of pH-induced conformational changes of biomacromolecules or synthetic polymers to modulate spatial proximity between the FRET pair. In addition, the introduction of pH-sensitive dyes in combination with pH-insensitive ones can also lead to the construction of ratiometric fluorescent pH probes. Larpent and co-workers[60] constructed ratiometric fluorescent pH probes based on core–shell type nanoparticles with the core physically encapsulated with a reference dye (1,9-diphenylanthracene, DPA) and the corona covalently labeled with fluorescein isothiocyanate (FITC). It is well-known that the FITC emission is highly dependent on solution pH, which decreases ~10–20 times in the pH range of 8–3. However, the fluorescence spectra need to be recorded at two excitation wavelengths to calculate emission intensity ratios. Scharff-Poulsen *et al.*[61] synthesized cross-linked polyacrylamide nanoparticles covalently attached with pH-sensing fluorescein and rhodamine B (RhB) as a reference dye; in this example, the dye loading contents were tuned to maximally avoid the FRET process between the two dyes and ratiometric pH sensing was again achieved by monitoring emission intensity ratios of fluorescein and RhB moieties excited at two maximum absorption wavelengths for the two types of dyes, respectively. Recently, Albertazzi and co-workers[27] reported the synthesis and subcellular targeted delivery of dendrimer-based fluorescent pH sensors, and the dendrimer periphery was functionalized with pH-insensitive dye (Rhodamine RedX) and one of three types of pH-sensitive dyes with varying pH response ranges, namely 7-hydroxy-4-coumarinylacetic acid, 5(6)-carboxyfluorescein, and Oregon Green 488. Both *in vitro* and *in vivo* ratiometric cellular pH sensing and imaging were then achieved.

It is worth noting that the above examples concerning polymeric ratiometric fluorescent pH probes typically involve a pH-sensitive dye (*e.g.*, FITC) and another pH-insensitive reference dye (*e.g.*, DPA or RhB). In principle, the possible occurrence of the FRET process from FITC to RhB within polymeric nanoparticles or dendrimers will weaken pH-induced changes in emission intensity ratios and decrease the signal contrast for subtle pH variations. Previously, we reported that rhodamine B-ethylenediamine derivative (RhBAM, see Scheme 1) exhibits pH-switchable characteristics.[23] It exists in the spirolactam form above pH 6 and exhibits no fluorescence emission, whereas below pH 6–7 it transforms into the acyclic form associated with ~8–10-fold increase of emission intensity in the range of pH 4–7. This property has been utilized by us to construct ratiometric

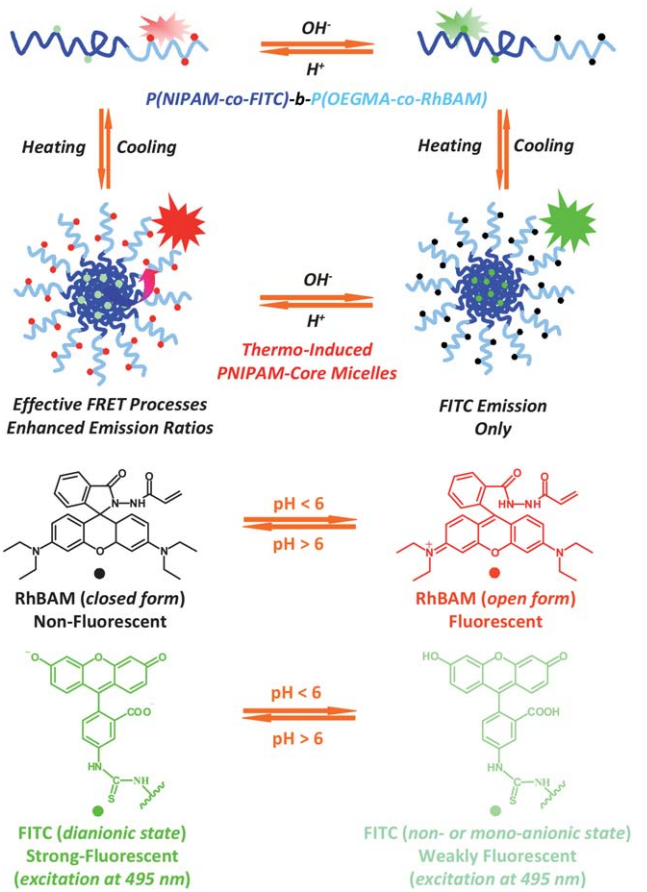

Scheme 1 Thermo- and pH-modulation of the fluorescence emissions of unimers and micelles of P(NIPAM-*co*-FITC)-*b*-P(OEGMA-*co*-RhBAM) DHBCs bearing FITC and RhBAM dyes with opposite pH-switchable emission characteristics in the thermoresponsive PNIPAM and hydrophilic POEGMA blocks, respectively.

fluorescent pH probes based on water-soluble random copolymers[22] and amphiphilic block copolymer micelles.[23] In both cases, a pH-insensitive dye, NBDAE, was used as the FRET donor and effective FRET processes occurred between NBDAE and RhBAM within the random copolymer chain or amphiphilic block copolymer micelles.

On the other hand, it is well-known that FITC is in the dianionic state with strong emission above ~pH 6, whereas below pH 6 it is in the non- or mono-anionic state associated with much weaker fluorescence.[62,63] Thus, fluorescence emissions of FITC and RhBAM moieties exhibit exactly opposite trends of changes with the increase or decrease of pH in the range of pH 4–7, which is of key relevance to the biological milieu. Considering the above drastically different pH-switchable emission characteristics of FITC and RhBAM moieties, we then speculate that the integration of the two types of dyes with pH-responsive diblock copolymers would provide extra advantages in terms of pH-detection sensitivity, as compared to previously reported pH-sensing polymeric probes involving a pH-sensitive dye and a reference dye.[22,23,27,60,61] In addition, the possible occurrence of FRET processes between FITC and acyclic RhBAM will further contribute to the changes in emission intensity ratios and signal contrast at intermediate pH ranges. Moreover, if thermoresponsive DHBCs with the two blocks respectively labeled with FITC and RhBAM moieties were employed as the sensing carrier, the FRET process between micellar cores and coronas can be facilely switched on and off *via* thermo-induced formation and dissociation of micelles, which can be utilized to modulate the pH detection sensitivity and integrate a fluorometric ratiometric pH-sensing function with a temperature-probing capability.

Based on the above considerations, herein, we report on the fabrication of highly sensitive and ratiometric fluorescent pH and temperature probes based on thermoresponsive DHBCs with the two blocks respectively labeled with two types of dyes possessing opposite pH-tunable emission characteristics (Scheme 1). P(NIPAM-*co*-FITC)-*b*-P(OEGMA-*co*-RhBAM) DHBCs were synthesized *via* consecutive reversible addition–fragmentation chain transfer (RAFT) polymerizations in combination with post-modification, where NIPAM and OEGMA are *N*-isopropylacrylamide and oligo(ethylene glycol) monomethyl ether methacrylate, respectively (Scheme 2).[64–67] Due to that FITC and RhBAM moieties exhibit a prominent decrease and increase in emission intensities with decreasing solution pH, respectively, intensity ratios of characteristic RhBAM and FITC emission bands, I_{582}/I_{522}, for P(NIPAM-*co*-FITC)-*b*-P(OEGMA-*co*-RhBAM) unimers at 25 °C exhibit ~39-fold changes in the pH range of 2–10. At elevated temperatures, thermo-induced formation of PNIPAM-core micelles enables effective FRET between FITC and RhBAM moieties located within micellar cores and coronas, respectively, and I_{582}/I_{522} exhibits ~52.5-fold changes in the same pH range. Compared to previously reported examples of fluorometric ratiometric polymeric pH probes,[22,23,27,60,61] the current design possesses the following improvements (Scheme 1): (1) instead of using a combination of pH-sensitive fluorescent dye and a reference dye, we employed two types of pH-sensitive dyes with their emission intensities exhibiting opposite pH-dependent trends, this will greatly enhance the pH-detecting sensitivity as much larger intensity ratio changes are involved accompanied with pH variations; (2) the two types of dyes were covalently labeled into the two blocks of a thermoresponsive diblock copolymer, thus, thermo-induced diblock micellization can effectively promote the FRET process between FITC and RhBAM located within micellar cores and coronas, as compared to that for diblock unimers, this has been confirmed to be capable of further enhancing pH-induced changes in emission intensity ratios and signal contrast; (3) finally, the use of thermoresponsive DHBC as the labeling matrix for the two types of dyes allows for the simultaneous and ratiometric fluorescent sensing of pH and temperature. Overall, the capability of multicolor-emitting P(NIPAM-*co*-FITC)-*b*-P(OEGMA-*co*-RhBAM) DHBCs for the ultrasensitive fluorometric detection of solution pH and temperature in a ratiometric manner augurs well for their practical applications in sensing, imaging, and combined diagnosis and therapy.

2. Experimental section

Materials

Oligo(ethylene glycol) monomethyl ether methacrylate (OEGMA, M_n = 475, mean degree of polymerization, DP, is 8–9; Aldrich) was passed through an alumina column to remove the inhibitor. *N*-Isopropylacrylamide (NIPAM, 97%, Tokyo Kasei Kagyo Co.) was recrystallized twice from a benzene/hexane mixture (1 : 3 v/v) prior to use. 2,2′-Azoisobutyronitrile (AIBN) was recrystallized from ethanol. *N*-(3-Aminopropyl) methacryl-amide hydrochloride (APMA) was purchased from Polysciences (98%) and used as received. Fluorescein isothiocyanate (FITC) was purchased from Aldrich (99%) and used as received. Rhodamine B-ethylenediamine derivative-based monomer, RhBAM,[23] and 4-cyano-4-(thiobenzoylthio)pentanoic acid[68] were synthesized according to literature procedures. All other chemicals were purchased from Sinopharm Chemical Reagent Co. and used as received.

Sample synthesis

Synthetic scheme employed for the RAFT synthesis of P(NIPAM-*co*-FITC)-*b*-P(OEGMA-*co*-RhBAM) and other control block copolymers is shown in Scheme 2. The structural parameters of P(OEGMA-*co*-RhBAM) precursor and the DHBCs are shown in Table S1.†

Synthesis of P(OEGMA-*co*-RhBAM) macroRAFT agent. Typical procedures employed for the synthesis of P(OEGMA-*co*-RhBAM)$_{90}$ precursor are as follows. OEGMA (5.71 g, 12 mmol), RhBAM (30.8 mg, 0.06 mmol), 4-cyano-4-(thiobenzoylthio)pentanoic acid (28 mg, 0.10 mmol), and AIBN (3.2 mg, 0.02 mmol) at a molar ratio of 600 : 3 : 5 : 1 were charged into a glass tube containing 6 mL 1,4-dioxane. The tube was then degassed *via* three freeze–pump–thaw cycles and flame-sealed under vacuum. It was then immersed into an oil bath thermostated at 70 °C to start the polymerization. After 8 h, the tube was quenched in liquid nitrogen to terminate the polymerization. The mixture was diluted with ethanol and purified by dialysis (Roth, ZelluTrans membrane, molecular weight cutoff: 4000–6000 Da) against a water/ethanol mixture (1 : 1 v/v). Subsequently, the solvents were removed by rotary evaporation.

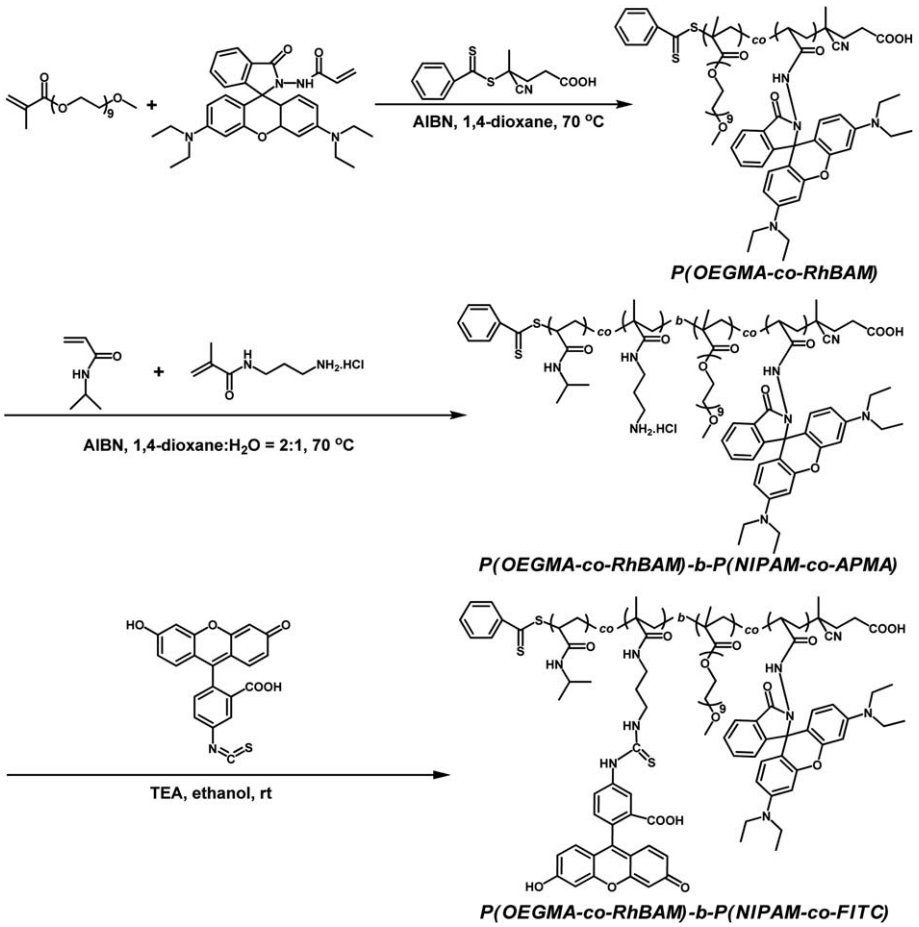

Scheme 2 A synthetic scheme employed for the RAFT synthesis of P(NIPAM-*co*-FITC)-*b*-P(OEGMA-*co*-RhBAM) double hydrophilic block copolymers with the thermoresponsive PNIPAM block and hydrophilic POEGMA block respectively labeled with FITC and rhodamine B-ethylenediamine (RhBAM) moieties possessing opposite pH-switchable emission characteristics.

The purified polymer appeared as a viscous solid (4.01 g, ~71% yield) and was dried in a vacuum oven overnight at room temperature. The molecular weight and molecular weight distribution of P(OEGMA-*co*-RhBAM) were determined by GPC using DMF as eluent ($M_n = 36\,200$, $M_w/M_n = 1.10$). The actual degree of polymerization (DP) of the P(OEGMA-*co*-RhBAM) was determined to be 90 by ^{1}H NMR analysis in $CDCl_3$. It was denoted as P(OEGMA-*co*-RhBAM)$_{90}$ and employed as the macroRAFT agent for the subsequent synthesis of P(NIPAM-*co*-APMA)-*b*-P(OEGMA-*co*-RhBAM) diblock copolymers. Following similar procedures, POEGMA$_{87}$ macroRAFT agent was also synthesized with an M_n of 35 100 and an M_w/M_n of 1.08 (Table S1†).

Synthesis of P(NIPAM-*co*-APMA)-*b*-P(OEGMA-*co*-RhBAM) diblock copolymers. In a typical example, P(OEGMA-*co*-RhBAM)$_{90}$ macroRAFT agent (1.72 g, 0.04 mmol), NIPAM (0.23 g, 2 mmol), APMA (7.1 mg, 0.04 mmol), AIBN (1.3 mg, 0.008 mmol), and 3 mL 1,4-dioxane/water mixture (2/1, v/v) were added into a glass ampoule. The mixture was degassed *via* three freeze–pump–thaw cycles and then flame-sealed under vacuum. The tube was immersed into an oil bath thermostated at 70 °C to start the polymerization. After 12 h, the tube was quenched in liquid nitrogen to terminate the polymerization. After removing all the solvents under reduced pressure, the residues were dissolved in THF and then precipitated into an excess of ethyl ether. This purification cycle was repeated twice. The final product was obtained as a pink solid after drying under vacuum overnight. The molecular weight and molecular weight distribution of P(NIPAM-*co*-APMA)-*b*-P(OEGMA-*co*-RhBAM)$_{90}$ diblock copolymer was determined by GPC using DMF as eluent: $M_n = 41\,500$, $M_w/M_n = 1.23$. The DP of PNIPAM block was determined to be 36 by ^{1}H NMR in $CDCl_3$. The obtained diblock copolymer was denoted as P(NIPAM-*co*-APMA)$_{36}$-*b*-P(OEGMA-*co*-RhBAM)$_{90}$. Following similar procedures, P(NIPAM-*co*-APMA)$_{34}$-*b*-POEGMA$_{87}$ was also synthesized and its structural parameters are summarized in Table S1.†

Synthesis of P(NIPAM-*co*-FITC)$_{36}$-*b*-P(OEGMA-*co*-RhBAM)$_{90}$ diblock copolymer. In a typical example, P(NIPAM-*co*-APMA)$_{36}$-*b*-P(OEGMA-*co*-RhBAM)$_{90}$ (0.415 g) was dissolved in a mixture of 20 mL ethanol and 0.05 mL triethylamine. FITC (4 mg, 10 μmol) in 0.5 mL ethanol solution was then added to the mixture at room temperature. After stirring overnight, the mixture was precipitated into an excess of anhydrous ethyl ether. This purification cycle was repeated twice. The product was obtained as an orange solid after drying under vacuum overnight. The molecular weight and molecular weight distribution of P(NIPAM-*co*-

FITC)$_{36}$-*b*-P(OEGMA-*co*-RhBAM)$_{90}$ diblock copolymer was determined by GPC using DMF as eluent: $M_n = 41\,700$, $M_w/M_n = 1.24$. The actual molar contents of FITC and RhBAM dye moieties within the diblock copolymer were quantified by absorption measurement against the standard calibration curve of free dyes. FITC content in the P(NIPAM-*co*-FITC)$_{36}$-*b*-P(OEGMA-*co*-RhBAM)$_{90}$ DHBC was determined by characteristic absorption at ~495 nm (pH 7). Note that the RhBAM moiety is in the spirolactam form under neutral and base conditions, which exhibits negligible absorbance. The RhBAM content in the DHBC was determined at pH 2 by employing the characteristic absorption of acyclic RhBAM moieties at ~565 nm. It was determined that, on average, one P(NIPAM-*co*-FITC)$_{36}$-*b*-P(OEGMA-*co*-RhBAM)$_{90}$ block copolymer chain contains ~0.72 FITC and ~0.49 RhBAM moieties. Following similar protocols, P(NIPAM-*co*-FITC)$_{34}$-*b*-POEGMA$_{87}$ was also synthesized and its structural parameters are also summarized in Table S1.†

Characterization

The temperature-dependent optical transmittance of the polymer aqueous solution at a wavelength of 700 nm was acquired on a Unico UV/vis 2802PCS spectrophotometer; a thermostatically controlled couvette was employed and the heating rate was 0.2 °C min^{-1}. The lower critical solution temperature (LCST) was defined as the temperature corresponding to ~1% decrease in optical transmittance. For the temperature-dependent turbidimetry experiments, polymer concentrations were fixed at 1.0 g L^{-1}. Dynamic laser light scattering (LLS) measurements were conducted on a commercial spectrometer (ALV/DLS/SLS-5022F) equipped with a multi-tau digital time correlator (ALV5000) and a cylindrical 22 mW UNIPHASE He-Ne laser ($\lambda_0 = 632$ nm) as the light source. Scattered light was collected at a fixed angle of 90° for duration of ~5 min. Distribution averages and particle size distributions were computed using cumulants analysis and CONTIN routines. All data were averaged over three measurements and the polymer concentrations were fixed at 0.3 g L^{-1}. Fluorescence spectra were recorded on a F-4600 (Hitachi) spectrofluorometer. The temperature of the water-jacketed cell holder was controlled by a programmable circulation bath. The slit widths were set at 5 nm for excitation and 5 nm for emission. For all fluorescence measurements, polymer concentrations were fixed at 0.1 g L^{-1}. Fluorescent images were taken on an Olympus IX71 fluorescence microscope equipped with a temperature-regulated incubator and a 450–480 nm exciter filter in combination with long pass 515 nm barrier filters.

3. Results and discussion

Synthesis and thermo-induced micellization of P(NIPAM-*co*-FITC)-*b*-P(OEGMA-*co*- RhBAM) DHBCs

P(NIPAM-*co*-FITC)$_{36}$-*b*-P(OEGMA-*co*-RhBAM)$_{90}$ bearing FITC moieties in the thermoresponsive PNIPAM block and RhBAM moieties in the hydrophilic POEGMA block was synthesized *via* consecutive RAFT polymerizations followed by post-functionalization (Scheme 2). P(OEGMA-*co*-RhBAM)$_{90}$ macroRAFT agent was synthesized at first *via* the RAFT copolymerization of OEGMA and RhBAM comonomers at a feeding molar ratio of 200 : 1. Previously, we reported the RAFT copolymerization of NIPAM and RhBAM monomers;[23] moreover, the controlled RAFT polymerization of OEGMA monomer and its copolymerization with other methacrylate and acrylamide monomers was also well-documented in literature reports. The subsequent RAFT copolymerization of NIPAM and APMA was then conducted by utilizing P(OEGMA-*co*-RhBAM)$_{90}$ as the macroRAFT agent.[69,70] The target block copolymer, P(NIPAM-*co*-FITC)$_{36}$-*b*-P(OEGMA-*co*-RhBAM)$_{90}$, was obtained by reacting amine moieties with a slight excess of FITC. For comparison, block copolymers labeled with a single type of dye moiety in the PNIPAM or POEGMA block, P(NIPAM-*co*-FITC)$_{34}$-*b*-POEGMA$_{87}$ and P(NIPAM-*co*-APMA)$_{36}$-*b*-P(OEGMA-*co*-RhBAM)$_{90}$ were also synthesized. Their structural parameters are summarized in Table S1 in the ESI.† The actual molar contents of FITC and RhBAM dye moieties within the diblock copolymer were quantified by fluorescence measurement against the standard calibration curve of free dye monomers. It was determined that, on average, one P(NIPAM-*co*-FITC)$_{36}$-*b*-P(OEGMA-*co*-RhBAM)$_{90}$ block copolymer chain contains ~0.7 FITC and ~0.48 RhBAM moieties.

In aqueous solution, P(NIPAM-*co*-FITC)$_{36}$-*b*-P(OEGMA-*co*-RhBAM)$_{90}$ diblock copolymer molecularly dissolves at room temperature and self-assembles into micelles at elevated temperatures owing to the well-known lower critical solution temperature (LCST) phase transition behavior of the PNIPAM block. Fig. 1a shows the temperature dependence of optical transmittance at 700 nm recorded for 1.0 g L^{-1} aqueous solution of P(NIPAM-*co*-FITC)$_{36}$-*b*-P(OEGMA-*co*-RhBAM)$_{90}$ diblock copolymer. The critical micellization temperature (CMT) of the diblock copolymer is determined to be ~39 °C, which is higher than the LCST of the PNIPAM homopolymer due to the introduction of the highly hydrophilic POEGMA block. Dynamic LLS analysis further revealed intensity-average hydrodynamic radii, $<R_h>$, of ~4 nm and 22 nm for 0.3 g L^{-1} aqueous solution of P(NIPAM-*co*-FITC)$_{36}$-*b*-P(OEGMA-*co*-RhBAM)$_{90}$ at 25 °C and 45 °C, respectively (see Fig. 1b).

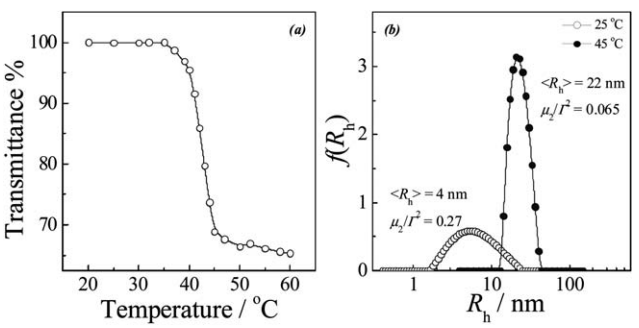

Fig. 1 (a) The temperature dependence of optical transmittance at 700 nm recorded for 1.0 g L^{-1} aqueous solution of P(NIPAM-*co*-FITC)$_{36}$-*b*-P(OEGMA-*co*-RhBAM)$_{90}$ diblock copolymer. (b) The hydrodynamic radius distributions, $f(R_h)$, recorded for 0.3 g L^{-1} aqueous solution of P(NIPAM-*co*-FITC)$_{36}$-*b*-P(OEGMA-*co*-RhBAM)$_{90}$ diblock copolymer at 25 °C and 45 °C, respectively.

P(NIPAM-*co*-FITC)-*b*-P(OEGMA-*co*-RhBAM) DHBC unimers and micelles as ratiometric pH and temperature probes

Previously, we reported that the RhBAM moiety within the hydrophilic PNIPAM corona of amphiphilic block copolymer micelles exists in the spirolactam form above ~pH 6 and is non-fluorescent; whereas below ~pH 6, it transforms into the acyclic form and emits strong fluorescence (Scheme 1).[23] In the current case, RhBAM dye monomers were copolymerized into the hydrophilic POEGMA block of DHBCs. At first, the fluorescence emission spectra were recorded for 0.1 g L^{-1} aqueous solution of the reference diblock copolymer without FITC labelling in the PNIPAM block, P(NIPAM-*co*-APMA)$_{36}$-*b*-P(OEGMA-*co*-RhBAM)$_{90}$, at varying pH (see Fig. S1 in the ESI†). With the decrease of the solution pH, the fluorescence intensity at 582 nm increased ~20 times when the solution pH decreased from 10 to 2 and most of the changes occurred below pH ~6. On the other hand, the protonation state of the carboxyl and phenolic moieties in the FITC derivative is highly dependent on the solution pH. It is in the dianionic state with quite strong fluorescence emission above pH 6, whereas below pH 6 it is in the non- or mono-anionic state associated with considerably weaker fluorescence emission (Scheme 1).[62,63] The pH-dependent fluorescence intensity changes of P(NIPAM-*co*-FITC)$_{34}$-*b*-POEGMA$_{87}$ reference diblock copolymer were then recorded. With the increase of pH in the range of 2–10, the fluorescence intensity at 522 nm increased ~14 times, and most of the increase occurred within the narrow pH range of 4–7 (see Fig. S2†). Thus, in the pH range of 2–10, the fluorescence emission of the FITC and RhBAM moieties exhibits exactly opposite pH-dependent changes, which dramatically increase and decrease with the solution pH. Most importantly, the observed pH-modulated changes in fluorescence emissions are fully reversible, as evidenced by the measurements of emission intensities when the solution pH was cycled between 3 and 7 (Fig. S3†).

Based on the above results, we speculate that when the two blocks of double hydrophilic block copolymers were appropriately labeled with FITC and RhBAM dye moieties, they should serve as highly sensitive ratiometric fluorescent pH probes. In the current case, one P(NIPAM-*co*-FITC)$_{36}$-*b*-P(OEGMA-*co*-RhBAM)$_{90}$ diblock copolymer chain contains ~0.7 FITC and ~0.48 RhBAM moieties. At 25 °C, which is below the CMT of the diblock copolymer, it will dissolve as isolated well-solvated random coils. Thus, the FRET process between FITC and acyclic RhBAM moieties at intermediate pH conditions will less possibly occur due to most of them being far apart from each other. However, due to their intrinsically different pH-dependent emission characteristics, diblock unimers will still serve as ultrasensitive ratiometric fluorescent pH probes.

Fig. 2 shows the fluorescence emission spectra and fluorescence intensity ratio changes excited at 495 nm, I_{582}/I_{522}, recorded for 0.1 g L^{-1} aqueous solution of P(NIPAM-*co*-FITC)$_{36}$-*b*-P(OEGMA-*co*-RhBAM)$_{90}$ diblock copolymer at 25 °C when the solution pH was decreased from 10 to 2. From Fig. 2a, we can apparently observe that with the decrease of pH, the emission intensity at 522 nm characteristic of FITC moieties decreased considerably, accompanied with the increase of the emission intensity at 582 nm characteristic

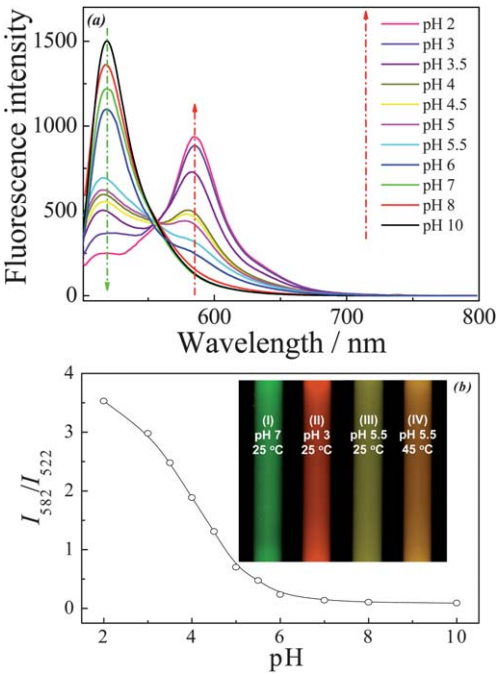

Fig. 2 (a) Fluorescence emission spectra and (b) fluorescence intensity ratio changes, I_{582}/I_{522}, recorded for 0.1 g L^{-1} aqueous solution of P(NIPAM-*co*-FITC)$_{36}$-*b*-P(OEGMA- *co*-RhBAM)$_{90}$ diblock copolymer (25 °C, λ_{ex} = 495 nm; slit widths: Ex. 5 nm, Em. 5 nm) in the pH range of 2–10. The inset in (b) shows optical photographs recorded for the aqueous solution of P(NIPAM-*co*-FITC)$_{36}$-*b*-P(OEGMA-*co*-RhBAM)$_{90}$ at (I) pH 7, 25 °C, (II) pH 3, 25 °C, (II) pH 5.5, 25 °C, and (IV) pH 5.5, 45 °C under an inverted fluorescence microscope equipped with a temperature-regulated incubator and 450–480 nm exciter filter in combination with a long pass 515 nm barrier filter.

of acyclic RhBAM moieties. The fluorescence intensity ratios, I_{582}/I_{522}, dramatically increased from ~0.09 to 3.5, *i.e.*, ~39-fold changes in emission ratios at 25 °C (see Fig. 2b). A closer examination of Fig. 2b further revealed that in the pH range of 7–4, which is the most biologically relevant, I_{582}/I_{522} exhibits ~14-fold changes. Previously, Scharff-Poulsen *et al.*[61] copolymerized pH-sensitive FITC and pH-insensitive RhB moieties into polyacrylamide microgels and reported that the emission intensity ratios exhibit ~6-fold changes in the pH range of 5.5–8.0. Moreover, in their case, the emission intensities of FITC and RhB were measured at two separate excitation wavelengths (488 and 543 nm), which is less convenient compared to the current system. The large pH-dependent changes in emission intensity ratios also lead the "naked-eye" detection of solution pH. As shown in the inset of Fig. 2b, we can clearly discern that the diblock unimer solution at 25 °C exhibits a fluorometric emission transition from green to yellowish and red when the solution pH decreases from 7 to 5.5, and 3.0, respectively.

We then further explored the pH detection capabilities of P(NIPAM-*co*-FITC)$_{36}$-*b*-P(OEGMA-*co*-RhBAM)$_{90}$ DHBC micelles formed at elevated temperatures (above the CMT). Theoretically, within micelles, FITC and RhBAM moieties are located within micellar cores and coronas, respectively; thus, they are in much closer spatial proximity (Scheme 1 and Fig. 1)

compared to diblock unimers below the CMT. It is well-accepted that the FRET efficiency between the two dyes is highly dependent on their spatial distances. Interestingly, when excited at 495 nm, the emission spectrum of FITC, ranging from 500 to 600 nm with a maximum at 522 nm, overlaps quite well with the absorption spectrum of the acyclic RhBAM moiety, which is in the range of 480–600 nm (see Fig. S4 in the ESI†). Thus, FITC and acyclic RhBAM moieties can construct an excellent FRET pair. Most importantly, the effective FRET process within micellar assemblies can further decrease and increase the emission intensity of FITC and RhBAM bands, respectively, and this will further enhance the pH-induced changes in emission intensity ratios.

To verify the above assumption, pH- and temperature-dependent fluorescence emission measurements for the aqueous solution of P(NIPAM-*co*-FITC)$_{36}$-*b*-P(OEGMA-*co*-RhBAM)$_{90}$ were further determined. We measured the temperature-dependent changes in fluorescence emissions and emission intensity ratios, I_{582}/I_{522}, at first for the diblock copolymer aqueous solution at an intermediate pH (pH 5.5), at which both FITC and RhBAM are emitting (Fig. 3). It was found that in the temperature range of 25–60 °C, the emission intensity at 522 nm exhibits a significant decrease, accompanied with the increase of the emission intensity band at 582 nm, and this clearly confirms the effects of thermo-induced diblock copolymer micellization on the FRET process. This conclusion is further evidenced from the fact that the most prominent changes in emission intensity ratios occur at temperatures around 40 °C, which reasonably agrees with the CMT of ~39 °C measured by temperature-dependent optical transmittance (Fig. 1a). Accordingly, the emission intensity ratios, I_{582}/I_{522}, increased from ~0.47 to ~1.68, *i.e.*, ~3.6-fold increase with the temperature increase from 25 to 60 °C. This also confirms that the diblock copolymer can also serve as ratiometric fluorescent temperature probes. From the inset in Fig. 2b, we can discern under fluorescence microscopy that the aqueous solution exhibits a fluorometric transition from yellowish to orange with the temperature increase from 25 to 45 °C.

To further confirm that the above observed thermo-induced changes in emission intensity ratios are mainly due to the enhanced FRET processes between FITC and acyclic RhBAM moieties located within micellar cores and coronas, we further measured the temperature-dependent fluorescence spectra of reference samples with only one the blocks labeled with relevant dyes, P(NIPAM-*co*-APMA)$_{36}$-*b*-P(OEGMA-*co*-RhBAM)$_{90}$ and P(NIPAM-*co*-FITC)$_{34}$-*b*-POEGMA$_{87}$ (Figs S5 and S6†). For both samples, their aqueous solutions exhibit ~1.11-fold and 1.46-fold increases in emission intensity, respectively, in the temperature range of 25–60 °C. This result clearly confirms that the FRET efficiency was dramatically enhanced in thermo-induced micelles associated with the considerable increase of the emission intensity ratios.

Based on the above results, we then probed the ratiometric pH-sensing performance of P(NIPAM-*co*-FITC)$_{36}$-*b*-P(OEGMA-*co*-RhBAM)$_{90}$ micelles. From Fig. 4, we can observe that in the pH range of 10–2 at 45 °C, the emission intensity ratio , I_{582}/I_{522}, exhibited ~52.5-fold increase, as compared to the ~39-fold enhancement for diblock unimers at 25 °C in the same pH range (Fig. 2b). It is worth noting that the increased temperature-dependent changes in fluorescence emission ratios for diblock copolymer micelles compared to unimers at elevated and low temperatures is highly relevant to the enhancement of pH-detection sensitivity and pH-imaging contrast. Overall, the aqueous solution of P(NIPAM-*co*-FITC)$_{36}$-*b*- P(OEGMA-*co*-RhBAM)$_{90}$ diblock copolymer exhibits multicolor emissions (see inset in Fig. 2b) depending on solution pH and temperatures, and it can serve as highly sensitive ratiometric fluorescent pH and temperature probes.

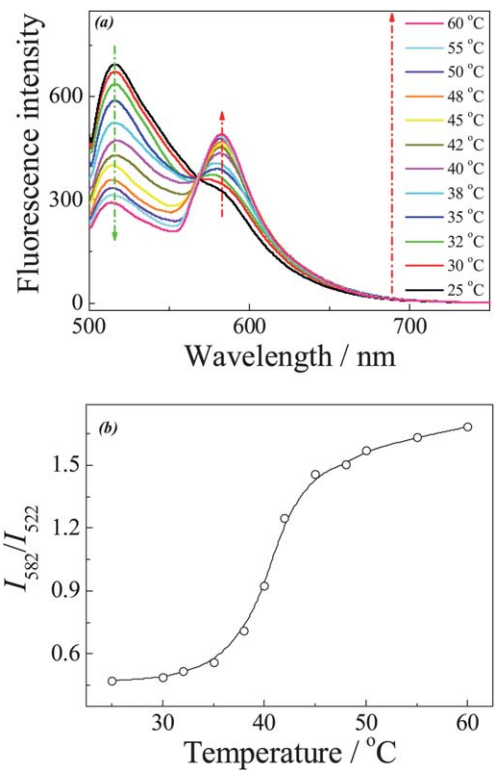

Fig. 3 (a) Fluorescence emission spectra and (b) fluorescence intensity ratio changes, I_{582}/I_{522}, recorded at varying temperatures in the range of 25–60 °C for 0.1 g L^{-1} aqueous solution of P(NIPAM-*co*-FITC)$_{36}$-*b*-P(OEGMA-*co*-RhBAM)$_{90}$ (pH 5.5, λ_{ex} = 495 nm; slit widths: Ex. 5 nm, Em. 5 nm).

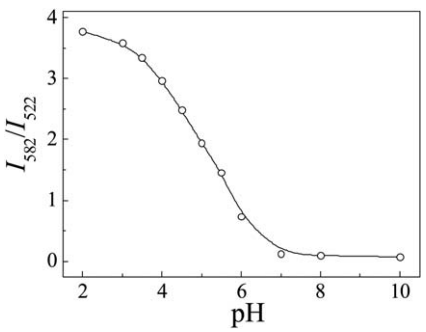

Fig. 4 Fluorescence intensity ratio changes, I_{582}/I_{522}, recorded for 0.1 g L^{-1} aqueous solution of P(NIPAM-*co*-FITC)$_{36}$-*b*-P(OEGMA-*co*-RhBAM)$_{90}$ diblock copolymer (45 °C, λ_{ex} = 495 nm; slit widths: Ex. 5 nm, Em. 5 nm) in the pH range of 2–10.

4. Conclusions

Highly sensitive ratiometric fluorescent pH and temperature probes based on thermoresponsive DHBCs with the two blocks labeled with two types of dyes possessing different pH-switchable emission characteristics were fabricated. P(NIPAM-*co*-FITC)-*b*-P(OEGMA-*co*-RhBAM) DHBCs were synthesized *via* RAFT polymerizations in combination with post-modification. Due to that FITC and RhBAM moieties exhibit prominent decreases and increases in emission intensities with decreasing solution pH, respectively, the intensity ratios of characteristic RhBAM and FITC emission bands, I_{582}/I_{522}, of diblock unimers at 25 °C exhibit ~39-fold changes in the pH range of 2–10. At elevated temperatures, thermo-induced formation of PNIPAM-core multimolecular micelles enables effective FRET between FITC and RhBAM moieties respectively located within micellar cores and coronas, and I_{582}/I_{522} exhibits ~52.5-fold changes in the same pH range. The reported dually modulated multicolor-emitting P(NIPAM-*co*-FITC)-*b*-P(OEGMA-*co*-RhBAM) DHBCs are capable of ultrasensitive fluorometric detection of solution pH and temperature in a ratiometric manner, which augurs well for their practical applications in sensing, imaging, and a new generation of theranostic systems.

Acknowledgements

The financial support from National Natural Scientific Foundation of China (NNSFC) Project (20874092, 91027026, and 51033005) and Fundamental Research Funds for the Central Universities is gratefully acknowledged.

References

1 P. D. Iddon and S. P. Armes, *Eur. Polym. J.*, 2007, **43**, 1234–1244.
2 C. L. Liu, C. H. Lin, C. C. Kuo, S. T. Lin and W. C. Chen, *Prog. Polym. Sci.*, 2011, **36**, 603–637.
3 Z. S. Ge, D. Xie, D. Y. Chen, X. Z. Jiang, Y. F. Zhang, H. W. Liu and S. Y. Liu, *Macromolecules*, 2007, **40**, 3538–3546.
4 A. E. Smith, X. W. Xu and C. L. Mccormick, *Prog. Polym. Sci.*, 2010, **35**, 45–93.
5 C. L. McCormick, S. E. Kirkland and A. W. York, *Polym. Rev.*, 2006, **46**, 421–443.
6 C. D. H. Alarcon, S. Pennadam and C. Alexander, *Chem. Soc. Rev.*, 2005, **34**, 276–285.
7 Y. L. Cai and S. P. Armes, *Macromolecules*, 2004, **37**, 7116–7122.
8 K. T. Kim, J. J. L. M. Cornelissen, R. J. M. Nolte and J. C. M. van Hest, *Adv. Mater.*, 2009, **21**, 2787–2791.
9 A. S. Lee, A. P. Gast, V. Butun and S. P. Armes, *Macromolecules*, 1999, **32**, 4302–4310.
10 A. Blanazs, S. P. Armes and A. J. Ryan, *Macromol. Rapid Commun.*, 2009, **30**, 267–277.
11 J. Xu and S. Y. Liu, *Soft Matter*, 2008, **4**, 1745–1749.
12 J. Kost and R. Langer, *Adv. Drug Delivery Rev.*, 2001, **46**, 125–148.
13 B. Jeong and A. Gutowska, *Trends Biotechnol.*, 2002, **20**, 305–311.
14 S. K. Ahn, R. M. Kasi, S. C. Kim, N. Sharma and Y. X. Zhou, *Soft Matter*, 2008, **4**, 1151–1157.
15 A. W. York, S. E. Kirkland and C. L. McCormick, *Adv. Drug Delivery Rev.*, 2008, **60**, 1018–1036.
16 J. M. Hu, C. H. Li and S. Y. Liu, *Langmuir*, 2010, **26**, 724–729.
17 J. M. Hu and S. Y. Liu, *Macromolecules*, 2010, **43**, 8315–8330.
18 S. Ganta, H. Devalapally, A. Shahiwala and M. Amiji, *J. Controlled Release*, 2008, **126**, 187–204.
19 H. N. Kim, Z. Q. Guo, W. H. Zhu, J. Yoon and H. Tian, *Chem. Soc. Rev.*, 2011, **40**, 79–93.
20 T. Liu and S. Y. Liu, *Anal. Chem.*, 2011, **83**, 2775–2785.
21 O. Onaca, R. Enea, D. W. Hughes and W. Meier, *Macromol. Biosci.*, 2009, **9**, 129–139.
22 X. J. Wan and S. Y. Liu, *J. Mater. Chem.*, 2011, **21**, 10321–10329.
23 C. H. Li, Y. X. Zhang, J. M. Hu, J. J. Cheng and S. Y. Liu, *Angew. Chem., Int. Ed.*, 2010, **49**, 5120–5124.
24 M. Onoda, S. Uchiyama and T. Ohwada, *Macromolecules*, 2007, **40**, 9651–9657.
25 H. Lomas, J. Z. Du, I. Canton, J. Madsen, N. Warren, S. P. Armes, A. L. Lewis and G. Battaglia, *Macromol. Biosci.*, 2010, **10**, 513–530.
26 J. M. Hu, L. Dai and S. Y. Liu, *Macromolecules*, 2011, **44**, 4699–4710.
27 L. Albertazzi, B. Storti, L. Marchetti and F. Beltram, *J. Am. Chem. Soc.*, 2010, **132**, 18158–18167.
28 Y. Y. Li, H. Cheng, J. L. Zhu, L. Yuan, Y. Dai, S. X. Cheng, X. Z. Zhang and R. X. Zhuo, *Adv. Mater.*, 2009, **21**, 2402–2406.
29 S. Modi, M. G. Swetha, D. Goswami, G. D. Gupta, S. Mayor and Y. Krishnan, *Nat. Nanotechnol.*, 2009, **4**, 325–330.
30 H. S. Peng, J. A. Stolwijk, L. N. Sun, J. Wegener and O. S. Wolfbeis, *Angew. Chem., Int. Ed.*, 2010, **49**, 4246–4249.
31 K. J. Zhou, Y. G. Wang, X. N. Huang, K. Luby-Phelps, B. D. Sumer and J. M. Gao, *Angew. Chem., Int. Ed.*, 2011, **50**, 6109–6114.
32 X. J. Wan, T. Liu and S. Y. Liu, *Langmuir*, 2011, **27**, 4082–4090.
33 B. B. Lowell and B. M. Spiegelman, *Nature*, 2000, **404**, 652–660.
34 L. E. Gerweck and K. Seetharaman, *Cancer Res.*, 1996, **56**, 1194–1198.
35 Y. Urano, D. Asanuma, Y. Hama, Y. Koyama, T. Barrett, M. Kamiya, T. Nagano, T. Watanabe, A. Hasegawa, P. L. Choyke and H. Kobayashi, *Nat. Med.*, 2009, **15**, 104–109.
36 A. S. E. Ojugo, P. M. J. McSheehy, D. J. O. McIntyre, C. McCoy, M. Stubbs, M. O. Leach, I. R. Judson and J. R. Griffiths, *NMR Biomed.*, 1999, **12**, 495–504.
37 J. Y. Han and K. Burgess, *Chem. Rev.*, 2010, **110**, 2709–2728.
38 D. M. Monti, L. Brandt, J. Ikomikumm and H. Olsson, *Scand. J. Haematol.*, 1986, **36**, 353–357.
39 M. Karnebogen, D. Singer, M. Kallerhoff and R. H. Ringert, *Thermochim. Acta*, 1993, **229**, 147–155.
40 C. Gota, K. Okabe, T. Funatsu, Y. Harada and S. Uchiyama, *J. Am. Chem. Soc.*, 2009, **131**, 2766–2767.
41 J. R. Casey, S. Grinstein and J. Orlowski, *Nat. Rev. Mol. Cell Biol.*, 2010, **11**, 50–61.
42 S. Charier, O. Ruel, J. B. Baudin, D. Alcor, J. F. Allemand, A. Meglio and L. Jullien, *Angew. Chem., Int. Ed.*, 2004, **43**, 4785–4788.
43 J. Yin, H. B. Hu, Y. H. Wu and S. Y. Liu, *Polym. Chem.*, 2011, **2**, 363–371.
44 J. Yin, C. H. Li, D. Wang and S. Y. Liu, *J. Phys. Chem. B*, 2010, **114**, 12213–12220.
45 D. Wang, T. Liu, J. Yin and S. Y. Liu, *Macromolecules*, 2011, **44**, 2282–2290.
46 S. Uchiyama and Y. Makino, *Chem. Commun.*, 2009, 2646–2648.
47 F. Mancin, E. Rampazzo, P. Tecilla and U. Tonellato, *Chem.–Eur. J.*, 2006, **12**, 1844–1854.
48 A. P. de Silva, S. Uchiyama, T. P. Vance and B. Wannalerse, *Coord. Chem. Rev.*, 2007, **251**, 1623–1632.
49 A. P. de Silva and S. Uchiyama, *Nat. Nanotechnol.*, 2007, **2**, 399–410.
50 S. Uchiyama, Y. Matsumura, A. P. de Silva and K. Iwai, *Anal. Chem.*, 2003, **75**, 5926–5935.
51 S. Uchiyama, Y. Matsumura, A. P. de Silva and K. Iwai, *Anal. Chem.*, 2004, **76**, 1793–1798.
52 C. Gota, S. Uchiyama and T. Ohwada, *Analyst*, 2007, **132**, 121–126.
53 K. Iwai, Y. Matsumura, S. Uchiyama and A. P. de Silva, *J. Mater. Chem.*, 2005, **15**, 2796–2800.
54 C. Gota, S. Uchiyama, T. Yoshihara, S. Tobita and T. Ohwada, *J. Phys. Chem. B*, 2008, **112**, 2829–2836.
55 S. W. Hong, D. Y. Kim, J. U. Lee and W. H. Jo, *Macromolecules*, 2009, **42**, 2756–2761.
56 B. L. Ma, M. Y. Xu, F. Zeng, L. F. Huang and S. Z. Wu, *Nanotechnology*, 2011, **22**, 065501.
57 S. Uchiyama, N. Kawai, A. P. de Silva and K. Iwai, *J. Am. Chem. Soc.*, 2004, **126**, 3032–3033.
58 C. Pietsch, R. Hoogenboom and U. S. Schubert, *Angew. Chem., Int. Ed.*, 2009, **48**, 5653–5656.
59 S. W. Hong, C. H. Ahn, J. Huh and W. H. Jo, *Macromolecules*, 2006, **39**, 7694–7700.
60 E. Allard and C. Larpent, *J. Polym. Sci., Part A: Polym. Chem.*, 2008, **46**, 6206–6213.
61 H. Sun, A. M. Scharff-Poulsen, H. Gu and K. Almdal, *Chem. Mater.*, 2006, **18**, 3381–3384.

62 E. Y. Bryleva, N. A. Vodolazkaya, N. O. Mchedlov-Petrossyan, L. V. Samokhina, N. A. Maveevskaya and A. V. Tolmachev, *J. Colloid Interface Sci.*, 2007, **316**, 712–722.
63 J. F. Peng, X. X. He, K. M. Wang, W. H. Tan, Y. Wang and Y. Liu, *Anal. Bioanal. Chem.*, 2007, **388**, 645–654.
64 L. Liu, C. L. Wu, J. C. Zhang, M. M. Zhang, Y. W. Liu, X. J. Wang and G. Q. Fu, *J. Polym. Sci., Part A: Polym. Chem.*, 2008, **46**, 3294–3305.
65 A. B. Lowe and C. L. McCormick, *Prog. Polym. Sci.*, 2007, **32**, 283–351.
66 A. E. Smith, X. W. Xu, S. E. Kirkland-York, D. A. Savin and C. L. McCormick, *Macromolecules*, 2010, **43**, 1210–1217.
67 X. W. Xu, J. D. Flores and C. L. McCormick, *Macromolecules*, 2011, **44**, 1327–1334.
68 S. H. Thang, Y. K. Chong, R. T. A. Mayadunne, G. Moad and E. Rizzardo, *Tetrahedron Lett.*, 1999, **40**, 2435–2438.
69 Y. Li, B. S. Lokitz and C. L. McCormick, *Angew. Chem., Int. Ed.*, 2006, **45**, 5792–5795.
70 Z. C. Deng, H. Bouchekif, K. Babooram, A. Housni, N. Choytun and R. Narain, *J. Polym. Sci., Part A: Polym. Chem.*, 2008, **46**, 4984–4996.

